Nanoscale

COMMUNICATION

View Article Online
View Journal | View Issue

Cite this: *Nanoscale*, 2015, **7**, 10963

Received 21st March 2015,
Accepted 29th May 2015

DOI: 10.1039/c5nr01818h

www.rsc.org/nanoscale

Drift-corrected nanoplasmonic hydrogen sensing by polarization†

Carl Wadell* and Christoph Langhammer*

Accurate and reliable hydrogen sensors are an important enabling technology for the large-scale introduction of hydrogen as a fuel or energy storage medium. As an example, in a hydrogen-powered fuel cell car of the type now introduced to the market, more than 15 hydrogen sensors are required for safe operation. To enable the long-term use of plasmonic sensors in this particular context, we introduce a concept for drift-correction based on light polarization utilizing symmetric sensor and sensing material nanoparticles arranged in a heterodimer. In this way the inert gold sensor element of the plasmonic dimer couples to a sensing-active palladium element if illuminated in the dimer-parallel polarization direction but not the perpendicular one. Thus the perpendicular polarization readout can be used to efficiently correct for drifts occurring due to changes of the sensor element itself or due to non-specific events like a temperature change. Furthermore, by the use of a polarizing beamsplitter, both polarization signals can be read out simultaneously making it possible to continuously correct the sensor response to eliminate long-term drift and ageing effects. Since our approach is generic, we also foresee its usefulness for other applications of nanoplasmonic sensors than hydrogen sensing.

Introduction

Plasmonic sensors have shown great promise in a large number of different areas, *e.g.* material science, catalysis, and chemosensing, which are in focus here.[1–4] The main reason for their success in such a wide range of fields stems from the fact that the Localized Surface Plasmon Resonances (LSPRs) in metallic nanoparticles are sensitive to many different processes occurring at the nano level, including changes in the properties of the sensor itself (material, size and shape); the dielectric environment around the sensor; and also temperature.[1,5] However, this strength is also one of their largest weaknesses in that it can be challenging to isolate the desired signal from other unwanted contributions. One way usually applied to tackle this problem is separate reference measurements on, *e.g.*, a blank sample and to subtract the two. However, often this does not fully solve the problem, since it is basically impossible to perform two completely identical measurements on two samples, with the only difference being the signal stemming from the process of interest. If applications in a real sensor device are targeted, it is furthermore very unpractical, if not impossible, to apply such a referencing strategy. Moreover, aging (changes of the sensor with time), temperature effects, as well as instabilities/drifts of the used light source and detector may become an issue and give rise to faulty readings when long-term use is targeted. This is critical in particular under harsh conditions in terms of temperature and chemical environment.

Here we present a simple, yet very effective, way to solve the aforementioned issues by using *simultaneous* readout of two light polarization signals from the same sample and simple subtraction of the two. In coupled plasmonic systems, polarization is a common way to interrogate different resonance modes.[6] Conceptually, separation of plasmonic modes using light polarization sensitive readout has previously been used for "self-referencing" to differentiate between surface-bound and bulk refractive index changes in plasmonic biosensors, by relying on a mathematical formalism and *asymmetric* nanostructures to achieve spectral mode splitting.[7,8]

We further advance this concept by demonstrating that with appropriate sample design and by relying on *symmetric* plasmonic sensor nanoparticles the measurement obtained in one polarization direction can be used efficiently to reference and drift-correct the sensor signal measured at the second polarization by means of simple signal subtraction, *i.e.* without the need for mathematical analysis. In other words, the actual measurement and the reference measurement can be carried out at the same time, in the same experiment and on the same spot on the sample. Furthermore, using a polarizing beamsplitter, the two polarization signals can be measured simultaneously making it possible to continuously correct the

Department of Applied Physics, Chalmers University of Technology, 412 96 Göteborg, Sweden. E-mail: carl.wadell@chalmers.se, clangham@chalmers.se

†Electronic supplementary information (ESI) available. See DOI: 10.1039/c5nr01818h

sensor readout in real time. This is of particular relevance for the emerging fields of nanoplasmonic sensing applications in materials science and catalysis,[1] as well as gas sensing,[4,9] where the plasmonic nanostructures are exposed to harsh chemical and thermal conditions over extensive periods of time and thus prone to signal artifacts due to unspecific changes of the sensor nanoparticles themselves.

We exemplify our approach on a plasmonic hydrogen sensor, which is motivated by the fact that with the recent market introduction of the first series-type hydrogen fuel cell cars,[10,11] and the prospect of a hydrogen economy at hand,[12] the development of safe and reliable hydrogen sensors becomes increasingly urgent. The wide flammability limits of hydrogen in air (4–75 vol%) in combination with low ignition energies makes fast and accurate detection of hydrogen leaks a vital part in any hydrogen driven vehicle but also in places where such vehicles are parked indoors, and in the necessary hydrogen infrastructure around them. Also in other contexts than a hydrogen economy scenario, hydrogen sensors are becoming increasingly important, for example in many industrial processes, in the food industry, and in health monitoring or disease diagnostics.[13–17]

The basic idea of our approach is to achieve the drift-correction functionality by organizing a plasmonic sensor element (here a Au nanoantenna) and an "active" analyte particle (here a small Pd nanoparticle that specifically interacts with hydrogen) in a "dimer"[18,19] fashion in such a way that only for one light polarization near field coupling between the sensor and active particle will occur. In contrast, for the second polarization no coupling occurs and changes to the active particle do *not* affect the LSPR of the sensor element but will only reflect changes occurring to the sensor element itself. Thus, signals related to ageing, temperature induced changes to the sensor element, non-specific events, light source fluctuations, *etc.* are easily accounted for and thus eliminated.

For this direct drift-correction approach to work, it is critical that the plasmonic response of the Au sensor elements (absolute amplitude of the shift) for the two polarizations is as similar as possible with regard to all changes except the ones occurring to the analyte particle. This means that the two resonances spectrally should be as close as possible since their response to, *e.g.*, dielectric changes strongly depends on their spectral position.[20,21] To achieve this we use *symmetric* plasmonic sensor elements (*i.e.* nanodisks) in contrast to earlier attempts using mode-splitting in rod-shaped plasmonic particles.[7] The symmetric sensor nanoparticle design has the further advantage that if any thermally induced shape changes occur during operation, these changes will take place with equal probability in all directions, *i.e.* in an isotropic way. Thus, it is more likely that they can be accounted for compared to a situation relying on asymmetric plasmonic particles.

Results and discussion

To demonstrate the working principle of our polarization-based drift-correction we present a plasmonic hydrogen sensor

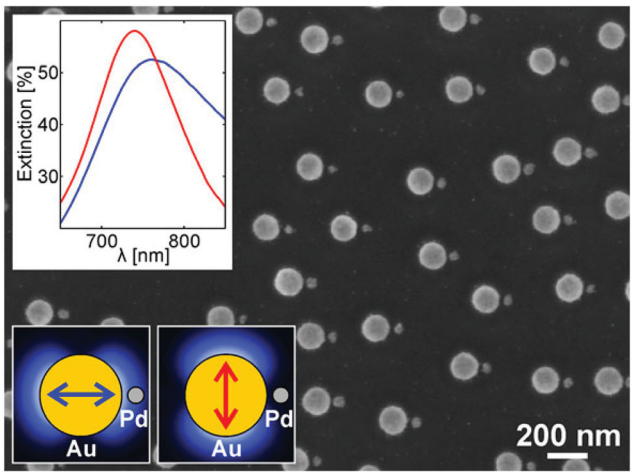

Fig. 1 Sketch of the drift-corrected nanoplasmonic hydrogen sensing principle with an SEM image of the used AuPd heterodimer structures in the background. The sensor consists of a quasi-random array of heterodimers featuring a large, inert disk-shaped Au sensor element (diameter 140 nm), and a small hydrogen-sensitive Pd particle (diameter 40 nm) fabricated next to it. The size-mismatch is chosen such that the LSPRs in the Au and Pd elements are significantly spectrally detuned. By the use of a polarizing beamsplitter the extinction spectra of polarizations parallel and perpendicular to the dimer axis are monitored simultaneously. The inset shows extinction spectra for the two polarizations, parallel (blue) and perpendicular (red). In the case of parallel polarization the Au disk plasmon couples to the Pd particle through its near field. For the perpendicular polarization the coupling is basically absent.

based on Au–Pd heterodimers (Fig. 1), where the hydride formation of Pd when exposed to hydrogen gas is used as model process to demonstrate the concept. As an important detail, we note that the Pd element size is chosen significantly smaller than the Au element to minimize spectral overlap of the respective LSPRs to reduce hybridization. We chose the Pd–H system as our model because it has been widely explored in the context of plasmonic hydrogen sensing,[3,4,22–25] and because the hydride formation process is both reversible and temperature dependent.[26] With this sensor design, as changes occur to the Pd particle upon interaction with hydrogen, they will mostly affect the LSPR of the Au sensor element if the structure is excited by light polarized parallel to the dimer axis. When excited in the perpendicular polarization direction, the Au sensor resonance will basically be unaffected.[27]

The samples are fabricated on glass substrates using shrinking-hole colloidal lithography (SHCL).[28] This is a self-aligned nanolithography technique based on the self-assembly of charged polystyrene nanospheres to form an evaporation mask, which facilitates the efficient patterning of large surface areas (cm^2) with the desired structures. At the same time, it also facilitates the independent accurate tuning of the size of the dimer elements. An overview SEM image of a typical sample surface is shown in Fig. S1 in the ESI.† The obtained surfaces allow for efficient ensemble extinction measurements using simple optics and polychromatic light. In particular, a polarizing beamsplitter was placed between the sample and

the spectrometer to simultaneously monitor both light polarizations, *i.e.* parallel and perpendicular to the dimer long axis. The principle is shown in Fig. 1, together with corresponding extinction spectra for the two light polarizations as indicated by the arrows.

For the hydrogen sensing experiments, the sample was mounted in a gas flow reactor where the atmosphere and temperature can be accurately controlled (for details see the Experimental section). The hydride formation and decomposition process in Pd can be induced by either changing the hydrogen concentration in the gas, or by changing the temperature of the sample at constant hydrogen concentration in the gas mixture. This makes it possible to study the sensor performance under either (i) constant temperature conditions and varied hydrogen concentration or (ii) at constant gas composition and varied temperature, respectively.

To really challenge and demonstrate the possibility for effective drift-correction we use freshly produced samples without subjecting them to any temperature pre-annealing. This is usually necessary to stabilize the sensor for operation at elevated temperature. If not preformed, large drifts in the signal will occur during the measurements due to recrystallization and reshaping effects of the nanostructures. Here we use these initial effects to "imitate" the effects of sensor aging over time and hence demonstrate the advantages of our drift-correction strategy.

Fig. 2 shows an experiment where the as-fabricated sample is first subjected to pulses of 4% hydrogen in Ar carrier gas at atmospheric pressure, followed by several temperature ramps from room temperature up to 100 °C in both pure Ar and Ar + H_2 mixtures. The blue and red curves in the top graph represent the shifts of the plasmon resonance peaks for the two different polarizations. Blue corresponds to the Au sensor element probing the Pd particle *via* near-field interaction (parallel polarization), and red to the uncoupled situation (perpendicular polarization). Both signals show distinct peak shifts during the course of the experiment, however the blue curve show features not visible in the red one. We now use the perpendicular (red) signal to drift-correct the sensor response, *i.e.* we take the difference between the two signals (blue minus red). The resulting corresponds to the green line in the graph. As the main result we find that the drift-corrected data now are only comprised of the peak shifts induced by the hydrogen sorption process in the Pd element, as induced by a change of H_2 concentration (first part), and by a change in temperature at constant H_2 concentration above the plateau pressure for hydride formation at room temperature (second part), as discussed in detail below. Most importantly we also notice only a minimal signal drift during the entire experiment after correction. The small still observed irreversible peak shift after the whole experiment is, however, to be expected since repeated hydrogen cycling will cause restructuring of the Pd particle caused by the lattice expansion induced during hydride formation before reaching a fully reversible equilibrium shape.[29] This restructuring can be seen clearly in the inset SEM images in Fig. 2, where the left image shows the

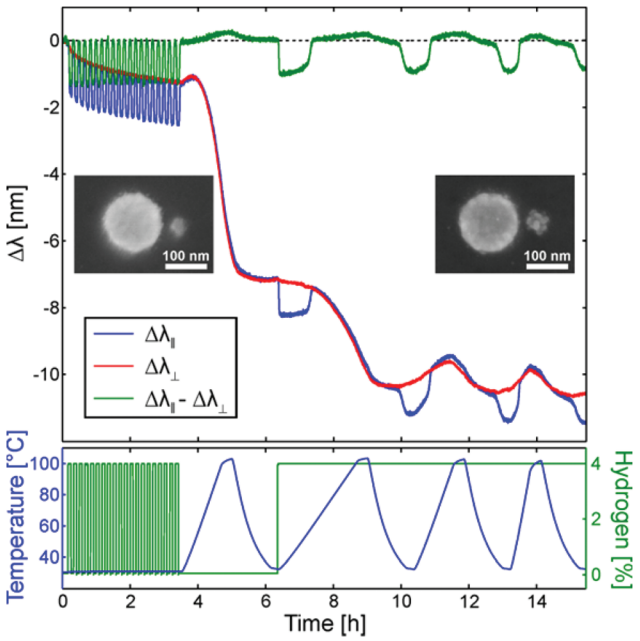

Fig. 2 The top graph shows the LSPR-peak response of the sensor for light polarization parallel to the dimer axis (blue), polarization perpendicular to the dimer axis (red), and the difference between the two (green). Note the almost perfect correction for long-term irreversible peak shifts in the drift-corrected (green) signal. The reshaping of the Pd particle induced by repeated hydride formation and decomposition, as seen in the two inset SEM images of the structures before (left) and after (right) the measurement, is the reason for the slight long-term signal drift that still is seen. Further cycling in hydrogen can be applied to completely eliminate this effect. The lower graph shows the temperatures (blue line) and hydrogen concentrations (green line) the sample was subjected to during the entire measurement sequence.

as fabricated sample and the right one the sample after the experiment.

We now take a more detailed look at the measurement shown in Fig. 2. Fig. 3 shows the first cycling sequence between 100% Ar and 4% H_2 in Ar (yellow shaded areas) at a constant temperature of 30 °C. At this temperature, 4% H_2 is enough to completely convert the Pd nanoparticle into its hydride phase (PdH_x).[22] This is what is seen in the LSPR signal from the Au sensor element measured in the parallel polarization configuration (blue line). As the hydrogen is introduced the resonance shifts ~1 nm to the blue. This shift is reversed as the hydride is decomposed again in pure Ar atmosphere. The observed shift is the result of two effects occurring during the hydride formation: (i) the change of the dielectric properties of the Pd particle as it is converted to PdH_x, and (ii) the aforementioned simultaneous volume expansion.[24–26] In addition, apart from the reversible hydride formation/decomposition steps, an irreversible long-term drift can be observed in the signal during the cycling. Comparing these observations with the response from the perpendicular polarization signal (red line) we notice that there are no steps observed during the PdH_x formation, whereas the long-term

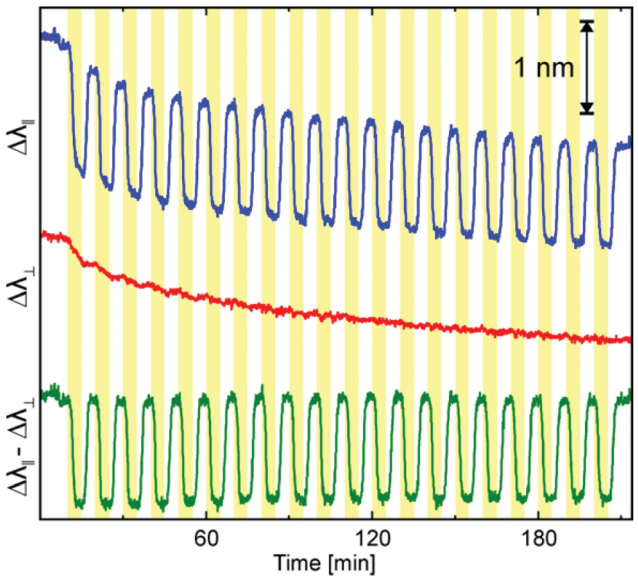

Fig. 3 Sensor response upon cyclic exposure to pure Ar (white shaded areas) and 4% H_2 in Ar (yellow shaded areas) at 30 °C. The blue line shows the LSPR peak response of the sensor upon excitation in the parallel polarization configuration, and the red line in the perpendicular polarization. The green line shows the difference between the two polarization signals and does not exhibit any drift or irreversibility over the 3.5 h duration of the experiment.

drift is present also here. This indicates that this irreversible long-term peak shift is not related to the actual hydride formation but is caused by changes occurring exclusively to the sensor element itself. The most likely explanation for this shift is desorption of species like water and hydrocarbons from the sensor surface in the dry atmosphere of the reactor. The fact that no discernible shift is observed upon hydrogen exposure moreover confirms that coupling between the Au sensor element and the Pd particle in the perpendicular polarization configuration is absent, and that possible contributions from higher order plasmonic modes in the Au elements are negligible in the analyzed range. Thus, we can indeed use the perpendicular polarization signal to correct for nonspecific long-term drift in the sensor readout by simply taking the difference between the two polarizations, as shown by the green line in Fig. 3.

In Fig. 4, which corresponds to the second temperature ramp in Fig. 2, the gas composition is kept constant at 4% H_2, which means that the Pd element is in the hydride phase at room temperature. At the same time the temperature is ramped linearly from 30 to 100 °C and then allowed to cool back to 30 °C. During the temperature increase, the PdH_x phase will decompose into Pd and hydrogen gas at a specific temperature. As the temperature is decreased, the hydride will be formed again as soon as the temperature is reduced below the equilibrium temperature. In other words, we will also here run a hydride formation/decomposition cycle but now using the temperature instead of a change in hydrogen concentration to induce the process. However, we also note that there typically is a distinct hysteresis in the formation decomposition process.[26,30] As before, the LSPR signal from the Au sensor element obtained for parallel polarization shows a clear response as the hydride is decomposed (*T*-increase) and formed again (*T*-decrease). However, this time a much more significant irreversible drift (~3 nm) is observed during the entire sequence. Since this shift is also observed in the perpendicular polarization signal (red), we conclude that it predominantly stems from changes to the sensor element itself (*e.g.* recrystallization that typically occurs upon a mild temperature treatment).[31] Moreover, during heating and cooling, a reversible peak shift of the Au sensor element is expected, predominantly due to lattice expansion-induced changes in electron density.[5] The latter is clearly seen in the third and forth temperature ramp sequence in Fig. 2 (as well as in detail in Fig. S2 in the ESI†) where the recrystallization process is terminated. Interestingly, even though these signals in sum are much larger than the one induced by the hydride formation/decomposition in the Pd element it is again possible to perfectly correct for them by simply taking the difference between the signals from the two polarizations. We also note that a small signature from the temperature increase still remains in the signal. This is evident from the first temperature ramp that was carried out in pure Ar atmosphere shown in Fig. 2 (as well as in detail in Fig. S3 in the ESI†). However, this is to be expected since the Pd particle itself also is affected by the temperature increase, *e.g.* through volume expansion. This will slightly alter the gap between the Au and Pd particles and therefore also the coupling between them, resulting in the small observed shift.

We can now go ahead and use the corrected signal to determine the hydride decomposition and formation temperatures at this hydrogen concentration, and derive an isobar. We do this by plotting the peak shift difference signal (green) *versus* temperature, as shown in the top right plot in Fig. 4. As evident from the figure, the drift correction has yielded a *fully reversible signal* that now shows all the characteristic features of the hydrogen sorption process in Pd:[22,26] (i) An α-phase with hydrogen in solid solution at low concentrations where the LSPR peak shift is small. (ii) A plateau region where the α- and hydride (β-) phase are in equilibrium and where the LSPR peak shift is large. (iii) A pure hydride phase region where the LSPR peak shift again is small. (iv) Distinct hysteresis between hydride formation and decomposition.

Another way to present this result is in the form as typically done for a temperature programmed desorption (TPD) measurement, that is, by plotting the first temperature derivative of the peak shift (obtained by a moving linear fit for a range of 5 °C) *versus* temperature.[32,33] As seen in the lower right plot in Fig. 4, for the increasing temperature ramp, this analysis yields a distinct peak at *ca.* 58 °C, which corresponds to the equilibrium temperature for the hydride decomposition at the given hydrogen partial pressure in the reactor. Any other features or signals are efficiently removed by the drift correction.

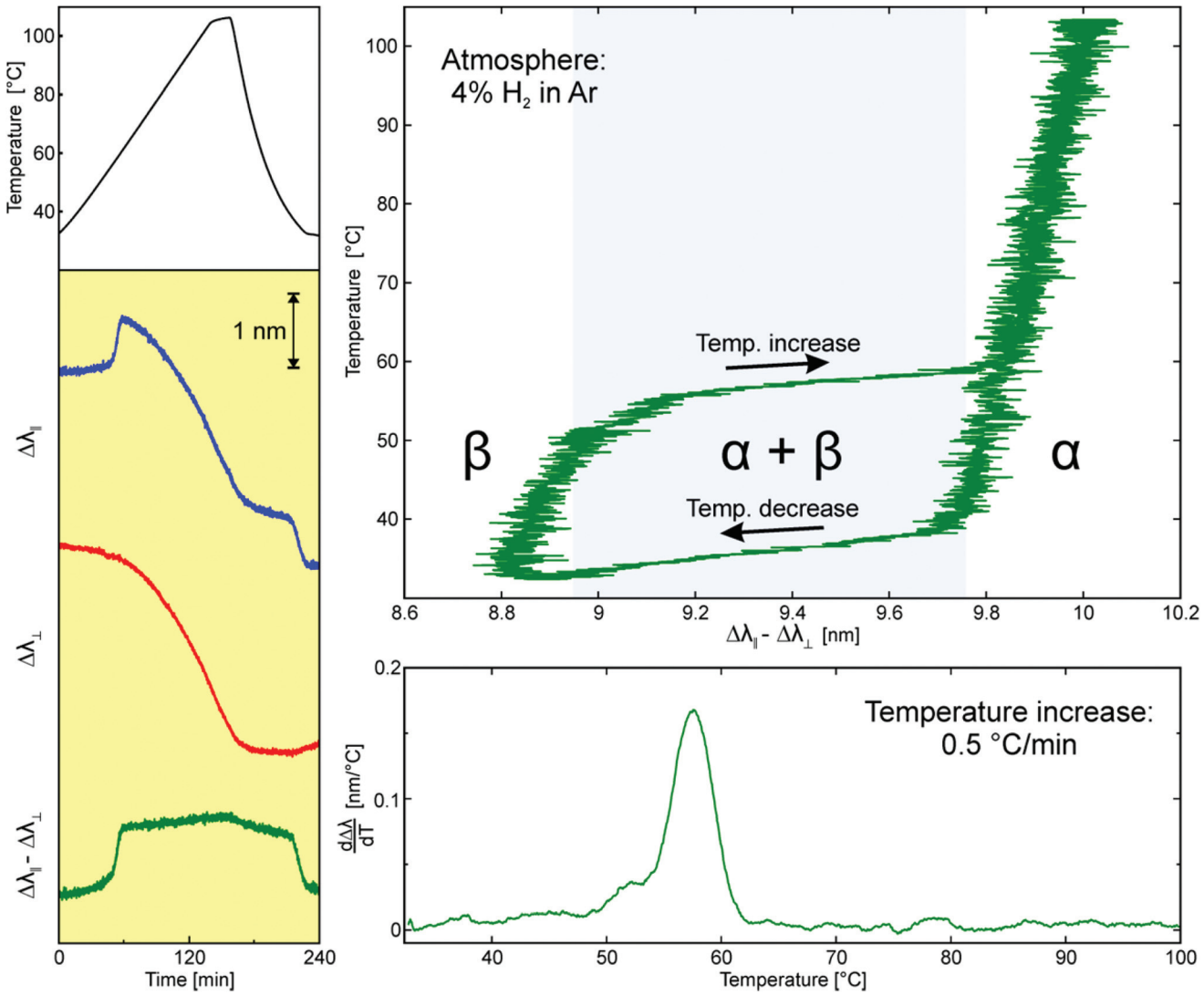

Fig. 4 Drift correction during a temperature ramp from 30 °C to above 100 °C in 4% H_2 in Ar. The top left graph shows the temperature ramp and the graph below shows the corresponding LSPR peak shifts measured in parallel (blue) and perpendicular (red) polarizations, as well as the difference (green) between the two. Notably, both the blue and red curves show significant irreversible peak shift (the reasons are discussed in the main text), whereas the difference signal is perfectly reversible and shows the following features: at the lower temperatures the Pd element is in the hydride phase (β-phase) until a critical temperature is reached where the hydride is decomposed into the α-phase (redshift). Upon cooling the opposite occurs, that is, below a critical temperature the hydride is formed again (blueshift). In the top right graph the difference signal is plotted *versus* the temperature of the sample, which yields a fully reversible isobar of the hydride decomposition and formation process in the Pd nanoparticle (note also the hysteresis between the decomposition and formation). The bottom right graph shows the numerical derivative of the isobar during the temperature increase (calculated using moving a linear fit with dT = 5 °C), yielding a signal similar to a temperature programmed desorption (TPD) measurement with a peak at the hydride decomposition temperature.

Experimental

Sample fabrication

The first steps in the shrinking-hole colloidal lithography process are the fabrication of an evaporation mask using hole-mask colloidal lithography.[28,34] All samples were fabricated on glass supports (Borofloat, Schott Scandinavia AB) or on a silicon wafer for the SEM imaging, according to the following chronological fabrication steps:

I. Substrates are cleaned by successive sonication in acetone, isopropanol and methanol, followed by rinsing in deionized (DI) water and blow-drying under an N_2 stream.

II. A sacrificial layer of poly(methyl methacrylate) (PMMA, MicroChem Corporation, 4 wt% diluted in anisole, MW = 950 000) is spin-coated onto the substrates for one minute at 2000 rpm and soft-baked on a hotplate at 170 °C for 10 minutes. This yields a PMMA film of ~280 nm thickness.

III. Samples are subjected to a short (5 s) oxygen plasma ash (50 W, 250 mTorr, Plasma Therm Batchtop RIE 95m) to increase the hydrophilicity of the PMMA surface.

IV. A polyelectrolyte solution (polydiallyldimethylammonium chloride (PDDA), MW = 200 000 ÷ 350 000, Sigma Aldrich, 0.2 wt% in Milli-Q water, Millipore) is pipetted on to the surface of the samples and incubated for 45 s before rinsing with DI water. This treatment makes the surface of the samples positively charged.

V. A colloidal suspension of negatively charged polystyrene (PS) particles with a mean diameter of 140 nm (sulfate latex, Interfacial Dynamics Corporation, 140 ± 5.18 nm, 0.2 wt% in Milli-Q water) is pipetted on to the surface of the samples and incubated for three minutes. Because of the negative surface charge on the PS particles they will spread out across the surface of the samples in a quasi-random array that is lacking long-range order. After removal of excess colloids by rinsing in DI water, the samples are blown dry under an N_2 stream.

VI. A 20 nm thick Au film is evaporated on top of the samples using an e-beam evaporation system (Lesker PVD 225) to form the hole-mask.

VII. Using a piece of tape (SWT-10, Nitto Scandinavia AB) the PS particles are stripped away from the surface of the samples leaving a Au film with holes at the former locations of the PS-particles.

VIII. The samples are exposed to an oxygen plasma treatment (7 minutes, 50 W, 250 mTorr, Plasma Therm Batchtop RIE 95m) to etch away the PMMA exposed below the holes in the Au film. Slightly longer etch times than what is needed to reach the bottom of the PMMA film are used to create an undercut below the Au mask that facilitates tilted evaporation through the mask.

IX. The samples are loaded in an e-beam evaporation system (Lesker PVD 225 Evaporator) with stage tilt possibility, and the following evaporations are made:

a. 20 nm Au at normal incidence
b. 100 nm Cr at normal incidence
c. 20 nm Pd at 17° off normal incidence

In our evaporation system this yields Au disks (diameter 140 nm) with a Cr cone on top and with smaller Pd disks (diameter ~40 nm) next to them.

X. The remaining PMMA layer is dissolved in acetone, removing the evaporation mask and only leaving the nanostructures on the sample surface.

XI. The samples are dipped in Cr etch (Sunchem AB, NiCr etchant 650095, composition: ceric ammonium nitrate 10–15%, nitric acid 15–20%, DI water 60–70%) for 1 minute, removing the Cr cone, but leaving the Au and Pd nanodisks in the targeted heterodimer arrangement.

Polarization dependent hydrogen sensing

The samples were mounted in a quartz tube flow reactor system with optical access (Insplorion X1, Insplorion AB, Göteborg, Sweden). Illumination of the sample is implemented *via* a fiber coupled halogen lamp (AvaLight-Hal-S, Avantes) and the polarization dependent extinction spectra are obtained using a polarizing beamsplitter (CM1-PBS252, Thorlabs) connected to two fiber-coupled spectrometers (AVASpec-1024, Avantes). LSPR peak positions for the two polarizations were obtained by fitting the measured extinction spectra with Lorentzian functions in the wavelength range of ±100 nm around the LSPR peak. The sample was initially subjected to pure Ar atmosphere with a flow of 100 ml min^{-1} and heated to 30 °C. As the temperature had stabilized the measurement shown in Fig. 2 was carried out. First, the sample was subjected to 20 cycles of hydrogen exposure at 4% H_2 in Ar carrier gas at atmospheric pressure. One cycle corresponds to five minutes in 4% H_2 followed by five minutes in pure Ar. At 30 °C, 4% H_2 is enough to completely transform the Pd into its hydride phase. In pure Ar the hydride is decomposed again. After these H_2 exposure cycles the sample was subjected to several linear heating and cooling cycles from 30 °C to 100 °C at different heating rates. The first cycle was carried out in Ar at a heating rate of 1 °C min^{-1}, followed by (after cooling in Ar to 30 °C) three heating/cooling cycles in 4% H_2 at heating rates of 0.5, 1, and 2 °C min^{-1}, respectively.

Conclusions

We have introduced a generic concept to correct for non-specific signals and long-term drift in nanoplasmonic sensors by using a polarizing beamsplitter and a tailored sample design. Specifically, we have developed a heterodimer nanoparticle arrangement comprised of an inert Au plasmonic sensor element and a hydrogen-sensitive Pd element specifically reacting with the analyte hydrogen gas. It was simultaneously probed by light polarized parallel and perpendicular to the dimer axis. In this way only for parallel polarization near field coupling between the Au sensor element and the active particle occurs and yields a signal induced by hydrogen sorption in the Pd element. The signal for perpendicular polarization measured simultaneously, only contains contributions from the sensor element itself or from light-source related instability and long-term drift. Therefore, it can efficiently be used to account for these unwanted signal contributions by simply subtracting it from the parallel polarization signal. Applying this approach to hydrogen sensing, we show that unspecific and unwanted contributions to the total sensor signal, stemming from processes like surface contaminant desorption, Au sensor element recrystallization, reversible temperature induced LSPR peak shifts, and lamp intensity fluctuations, can efficiently be accounted for, so that the pure hydrogen sorption process in the Pd element can be unveiled.

At the more general level, we highlight that the introduced drift-correction concept is generic and thus generally applicable to systems in which the specific interaction of an analyte can be controlled to only occur on a tailored active "spot" or particle in a heterodimer (or multimer) plasmonic sensor arrangement. We foresee that drift and fluctuation correction as demonstrated here (which, in principle, can be implemented also at the single particle plasmonic sensing

level) are critical ingredients to long term stability and reliability of plasmonic sensors in real applications, as well as in the quest towards single molecule detection.

Acknowledgements

We acknowledge financial support from the Swedish Research Council, the Swedish Foundation for Strategic Research Framework Program RMA11-0037, the Chalmers Area of Advance for Nanoscience and Nanotechnology, the Knut and Alice Wallenberg Stiftelse for their support of the infrastructure in the MC2 nanofabrication laboratory at Chalmers, and the Swedish Research Council for their support of the μ-fab cleanroom infrastructure in Sweden.

Notes and references

1 E. M. Larsson, S. Syrenova and C. Langhammer, *Nanophotonics*, 2012, **1**, 249–266.
2 E. M. Larsson, C. Langhammer, I. Zoric and B. Kasemo, *Science*, 2009, **326**, 1091–1094.
3 N. Liu, M. L. Tang, M. Hentschel, H. Giessen and A. P. Alivisatos, *Nat. Mater.*, 2011, **10**, 631–636.
4 C. Wadell, S. Syrenova and C. Langhammer, *ACS Nano*, 2014, **8**, 11925–11940.
5 O. A. Yeshchenko, I. S. Bondarchuk, V. S. Gurin, I. M. Dmitruk and A. V. Kotko, *Surf. Sci.*, 2013, **608**, 275–281.
6 N. J. Halas, S. Lal, W. S. Chang, S. Link and P. Nordlander, *Chem. Rev.*, 2011, **111**, 3913–3961.
7 N. Nehru, E. U. Donev, G. M. Huda, L. L. Yu, Y. N. Wei and J. T. Hastings, *Opt. Express*, 2012, **20**, 6905–6914.
8 N. Nehru, L. L. Yu, Y. N. Wei and J. T. Hastings, *IEEE Trans. Nanotechnol.*, 2014, **13**, 55–61.
9 A. Tittl, H. Giessen and N. Liu, in *Nanophotonics*, 2014, vol. 3, pp. 157–180.
10 Hyundai, ix35 Fuel Cell, http://worldwide.hyundai.com/WW/Showroom/Eco/ix35-Fuel-Cell/PIP/index.html, 2015.
11 Toyota, Fuel Cell Vehicle, http://www.toyota-global.com/innovation/environmental_technology/fuelcell_vehicle/, 2015.
12 A. Züttel, A. Borgschulte and L. Schlapbach, *Hydrogen as a future energy carrier*, Wiley-VCH, Weinheim, 2008.
13 R. B. Gupta, *Hydrogen fuel: production, transport and storage*, CRC Press, Boca Raton, 2009.
14 J. R. Wilkins, G. E. Stoner and E. H. Boykin, *Appl. Microbiol.*, 1974, **27**, 949–952.
15 C. H. S. Hitchcock, *J. Sci. Food Agric.*, 2000, **80**, 131–136.
16 E. U. Hurme and R. Ahvenainen, *J. Food Prot.*, 1998, **61**, 1165–1169.
17 W. Shin, *Anal. Bioanal. Chem.*, 2014, **406**, 3931–3939.
18 A. W. Clark and J. M. Cooper, *Angew. Chem., Int. Ed.*, 2012, **51**, 3562–3566.
19 H. Lee, J. H. Lee, S. M. Jin, Y. D. Suh and J. M. Nam, *Nano Lett.*, 2013, **13**, 6113–6121.
20 E. M. Larsson, J. Alegret, M. Kall and D. S. Sutherland, *Nano Lett.*, 2007, **7**, 1256–1263.
21 K. M. Mayer and J. H. Hafner, *Chem. Rev.*, 2011, **111**, 3828–3857.
22 I. Zoric, E. M. Larsson, B. Kasemo and C. Langhammer, *Adv. Mater.*, 2010, **22**, 4628–4633.
23 C. Langhammer, E. M. Larsson, B. Kasemo and I. Zoric, *Nano Lett.*, 2010, **10**, 3529–3538.
24 A. Tittl, C. Kremers, J. Dorfmuller, D. N. Chigrin and H. Giessen, *Opt. Mater. Express*, 2012, **2**, 111–118.
25 M. A. Poyli, V. M. Silkin, I. P. Chernov, P. M. Echenique, R. D. Muino and J. Aizpurua, *J. Phys. Chem. Lett.*, 2012, **3**, 2556–2561.
26 Y. Fukai, *The metal-hydrogen system*, Springer-Verlag, 2005.
27 T. J. Antosiewicz, S. P. Apell, V. Claudio and M. Kall, *Opt. Express*, 2012, **20**, 524–533.
28 S. Syrenova, C. Wadell and C. Langhammer, *Nano Lett.*, 2014, **14**, 2655–2663.
29 C. Langhammer, I. Zoric and B. Kasemo, *Nano Lett.*, 2007, **7**, 3122–3127.
30 R. B. Schwarz and A. G. Khachaturyan, *Phys. Rev. Lett.*, 1995, **74**, 2523–2526.
31 J. C. Tinguely, I. Sow, C. Leiner, J. Grand, A. Hohenau, N. Felidj, J. Aubard and J. R. Krenn, *BioNanoScience*, 2011, **1**, 128–135.
32 F. J. Castro and G. Meyer, *Rev. Sci. Instrum.*, 2000, **71**, 2131–2133.
33 F. J. Castro, G. Meyer and G. Zampieri, *J. Alloys Compd.*, 2002, **330–332**, 612–616.
34 H. Fredriksson, Y. Alaverdyan, A. Dmitriev, C. Langhammer, D. S. Sutherland, M. Zaech and B. Kasemo, *Adv. Mater.*, 2007, **19**, 4297–4302.